Paper **CFDSC2012-XX**,
20th Annual Conference of the CFD Society of Canada,
Canmore, Canada, May 9-12, 2012.

Numerical Simulations of Self-Sustained Pitch-Heave Oscillations of a NACA0012 Airfoil

Simon Lapointe and Guy Dumas[1]

Laboratoire de Mécanique des Fluides Numérique, Département de Génie Mécanique, Université Laval, Québec, G1V 0A6, Canada

Email: *simon.lapointe.5@ulaval.ca*

Abstract

The phenomenon of self-sustained pitch-heave oscillations of an airfoil at transitional Reynolds numbers is studied by two-dimensional numerical simulations using the Spalart-Allmaras and $\gamma - \mathrm{Re}_\theta$ models. Predicted pitching and heaving amplitudes and frequencies of the oscillations are compared with previous experimental results. The numerical simulations reproduce the same trends as in the experiments. When large translational stiffnesses are used, large heaving and pitching amplitudes are obtained. These oscillations can be labelled as coalescence flutter. The flow dynamics and the impact of the different turbulence models are also discussed.

1 Introduction

Over the course of the last decades, there has been an increasing interest in the development of unmanned aerial vehicles (UAVs) and micro-air vehicles (MAVs). These vehicles can be used in a large variety of applications and can be either remotely piloted or autonomous. As typical commercial aircrafts usually fly at high Reynolds number $O(10^7)$, the small length scale and low velocities of UAVs and MAVs result in a flight regime with low-to-moderate chord Reynolds numbers (15,000 to 500,000) [6].

The flow at these Re numbers is highly nonlinear and complex viscous phenomena are present. Indeed, one can typically observe an extensive region of laminar flow in the boundary layer up to the separation point. A transition of the laminar shear layer then follows with a possible re-attachment of the turbulent shear layer thus forming a laminar separation bubble (LSB) on the surface of the airfoil [1, 12].

Poirel's group [8] at Kingston has worked on a series of experimental studies on an elastically mounted NACA0012 wing at Reynolds numbers in the range $5.0 \times 10^4 < \mathrm{Re}_c < 1.2 \times 10^5$. Wind tunnel experiments have shown that the rigid airfoil in this transitional flow regime undergoes self-sustained or limit-cycle oscillations (LCO). Typical results are shown in Fig. 1. The pitch-only oscillations are characterized by a simple harmonic motion of small amplitudes (less than 5.5 deg) and nondimensionnal frequencies of the order $fc/U_\infty \approx 0.05 \sim 0.07$. These have also been observed numerically in different studies [4, 9] led at the CFD lab LMFN at Laval University. These oscillations have been labelled as laminar separation flutter since laminar boundary-layer separation is key to triggering the phenomenon and turbulent boundary layers inhibit the appearance of oscillations.

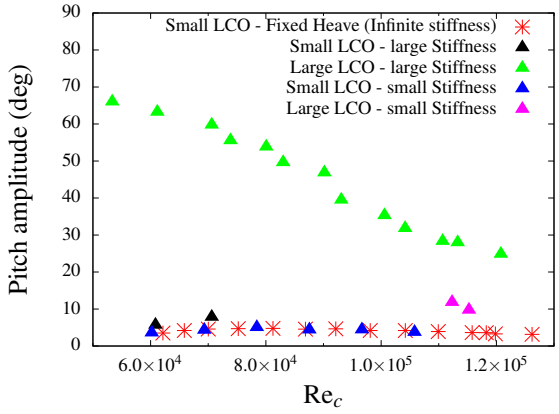

Figure 1: Comparison of self-sustained 2 DOF oscillations characteristics from experiments [5].

In their recent work, Mendes *et al.* [5] conducted wind tunnel experiments of a NACA0012 allowing two-degree-of-freedom motion in both the pitching and heave directions. Their experimental setup is illustrated in Fig. 2. The wing has a chord of 0.156m and a

span of 0.61m ($AR = 3.9$). The motion is permitted by the use of springs wrapped around two sets of pulleys. One pair of pulleys is attached to a rod at $0.186c$ from the leading edge of the airfoil to allow for the pitching motion. These springs have a stiffness of 58 N/m that is kept constant in all experiments. The heaving motion is constrained by another pulley system. Different stiffnesses were tested for the plunging springs: a low stiffness of 75 N/m and a high stiffness of 371 N/m.

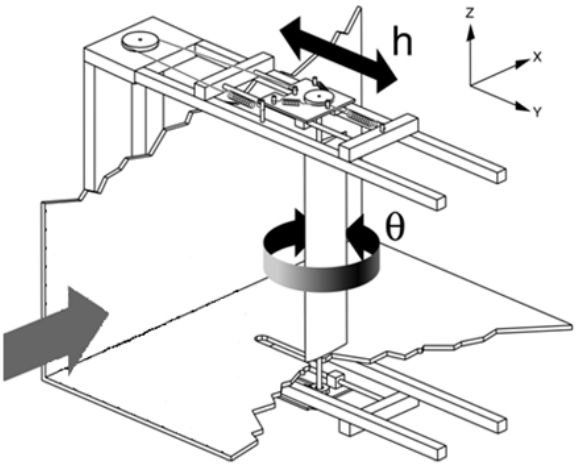

Figure 2: Schematic of experimental apparatus, reproduced from [5].

The two-degrees-of-freedom experimental results are also included in Fig. 1. Two types of oscillating amplitudes were observed: small and large. Although both small and large oscillations were measured using a high plunge stiffness, only small oscillations were obtained when a low plunge stiffness was used. In this case, the addition of a trip wire close to the leading edge did not inhibit the appearance of the large oscillations meaning that these large oscillations are not associated with laminar separation flutter but rather with coalescence flutter. Coalescence flutter is known as a dynamic instability leading to exponentially growing oscillations until aerodynamic or structural forces impede this growth creating the LCO behavior [5]. The instability responsible for the flutter occurs through the coupling effect between the pitching and heaving motions [10].

This paper aims to demonstrate the capability of modern CFD to capture and reproduce the observed complex coupling between the flow and the elastic structure.

2 COMPUTATIONAL METHODOLOGY

The fluid problem is solved with the finite volume, open source, CFD code *OpenFOAM* [7]. The fluid flow is governed by the mass and momentum conservation equations which take the following forms for an incompressible turbulent flow:

$$\frac{\partial U_i}{\partial x_i} = 0 \,, \tag{1}$$

$$\frac{\partial U_i}{\partial t} + U_j \frac{\partial U_i}{\partial x_j} = -\frac{1}{\rho}\frac{\partial p}{\partial x_i} + (\nu + \nu_t)\frac{\partial^2 U_i}{\partial x_j^2} \,, \tag{2}$$

where U is the ensemble averaged mean fluid velocity vector, ρ is the fluid density, p is the pressure, ν is the kinematic viscosity and ν_t is the turbulent kinematic viscosity. The fluid solver implements Eqs. (1) and (2) using the finite-volume method. The transient term is discretized with a second order backward implicit scheme. The convection term is discretized with a second order scheme based on a linear upwind interpolation. The diffusion term is discretized with a second order accurate scheme based on linear interpolation and using an explicit non-orthogonal-corrected surface normal gradient scheme. The pressure-velocity coupling is done by means of the PISO segregated algorithm. The linear solver is a preconditioned bi-conjugate gradient (PBiCG) method for the momentum and turbulence equations, and a generalised geometric-algebraic multi-grid (GAMG) method is used for the pressure equation.

The aeroelastic system corresponding to the experiments [5] is represented in the sketch of Fig. 3 along with the nominal parameters used in both the experiments and the numerical simulations. The freestream velocity U_∞ varies from 5 to 14 m/s.

A timestep of $\Delta t = 2 \times 10^{-5}$ sec has been used in all simulations. This allows for about $15,000$ timesteps per aeroelastic oscillation and 200 timesteps per vortex shedding period which has been verified to be quite sufficient. An RMS convergence criterion of 10^{-6} on all quantities is requested at each timestep. Timestep and convergence level independance studies have shown that using a finer timestep of $\Delta t = 1 \times 10^{-5}$ sec or reaching a convergence level of 10^{-7} did not change the results.

Fairly periodic oscillation cycles are observed and several such periodic cycles are computed to allow for the production of good, stationary statistics and spectral analysis. The typical run time for a whole simulation requires about one week on four Intel Xeon X5560 2.8 Ghz processors.

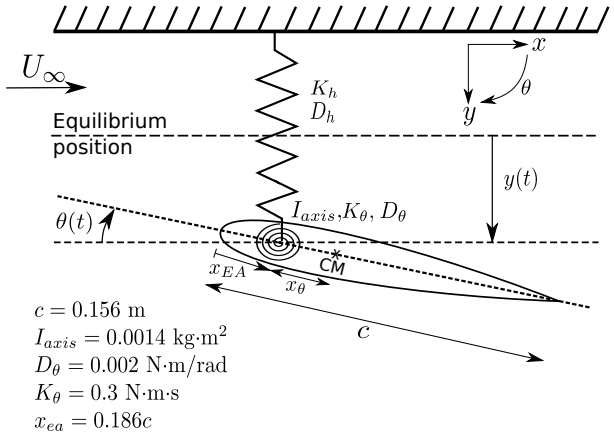

Figure 3: Two degrees of freedom aeroelastic modeling.

2.1 Aeroelastic modeling

We consider an elastically-mounted rigid body with two-degrees-of-freedom respectively in pitch and heave. The problem is sketched in Fig. 3. A Cartesian coordinate system is used with the y axis defined positive downward and the x axis positive towards the right, in order to respect the aerodynamic convention concerning the sign of the pitching angle θ.

The dynamics of the airfoil is thus governed by:

$$M_{axis} = I_{axis}\ddot{\theta} + D_\theta\dot{\theta} + K_\theta\theta + m\ddot{y}x_\theta cos(\theta) \quad (3)$$

$$-\mathcal{L} = m[\ddot{y} + x_\theta cos(\theta)\ddot{\theta} - x_\theta sin(\theta)\dot{\theta}^2] + D_y\dot{y} + k_y y. \quad (4)$$

where I_{axis} is the moment of inertia about the elastic axis, D_θ is the rotational damping coefficient, K_θ is the torsional stiffness coefficient, M_{axis} is the moment about the axis exerted by the fluid, m is the mass, D_y is the plunging damping coefficient, K_y is the plunging stiffness coefficent and $\mathcal{L}$ is the lift. The structural parameters indicated in Fig. 3 were obtained in the laboratory by direct physical measurements and from no-flow free decay tests [5, 8]. These equations are coupled in the general case where the pitching axis is not coincident with the center of mass ($x_\theta \neq 0$). In this paper $x_\theta = 0.1c$.

In the simulations, the flow solver is coupled with the dynamics of the elastically mounted rigid airfoil. The calculation algorithm, performed at each timestep, goes as follows:

1. The instantaneous fluid flow around the airfoil is computed;

2. The lift and moment exerted by the flow on the airfoil are calculated;

3. The equations of motion, Eq. (3) and (4), are solved using a fifth-order Runge-Kutta scheme to determine the pitch rate $\dot{\theta}$, angular position θ, vertical velocity $\dot{y}$ and position y;

4. The vertical and angular positions and velocities of the airfoil are thus updated and the next timestep can proceed.

2.2 Turbulence modeling

In the present study, turbulence closure is achieved by the Boussinesq eddy-viscosity approximation and the eddy viscosity ν_t is modeled by the Spalart-Allmaras RANS model [11] or the $\gamma - \mathrm{Re}_\theta$ transition model [3]. The S-A model is a one-equation turbulence model for the modified turbulent viscosity $\tilde{\nu}$. This model does not need wall functions since it provides near-wall resolution and is based on empiricism and arguments from dimensional analysis. Since simulations are performed at transitional Reynolds numbers, the $\gamma - \mathrm{Re}_\theta$ model is also tested to investigate the impact of the transition phenomena. It is a correlation-based transition model built on transport equations using only local variables. It adds two transport equations to the $k - \omega$ SST model.

Previously published comparisons of URANS calculations (algebraic, one-equation and two-equations turbulence models) with experimental measurements for pitching only (rotorcraft-type) oscillating airfoils indicated that the main weakness of the computational and theoretical methods was the turbulence modeling [2]. It is already known that unsteady calculations may be strongly affected by the choice of turbulence and transition models [13]. Although the Spalart-Allmaras model has been built up based on aerodynamic considerations, it was developed from steady flow cases and shares the same basic limitations as other RANS models for flows characterized by massive separation. URANS turbulence modeling is thus obviously challenged here and may be criticized. However, it is important at this point to recall that the current paper objective is not so much to provide precise quantitative results for the entire parametric space, but to give basic insights into the complex unsteady flow physics of self-sustained oscillating airfoils.

Despite the uncertainty of the quantitative predictions for massively separated flows, we argue that the current URANS study is nonetheless of significant practical interest as it provides the right physical trends and thus, useful physical insights for the first time ever as far as the author knows.

2.3 Boundary conditions and space discretization

The pitch-heave oscillating airfoil problem is here solved in an accelerated translational frame of reference which thus requires moving body and moving grid capabilities to simulate the pitching motion.

In *OpenFOAM*, a non-conformal interface can be used in order to avoid deforming mesh and remeshing in the close proximity of the airfoil. To take into account the pitching motion, the inner part of the mesh, located inside a radius of 2 chords about the pitching axis, rotates rigidly with the body while the outer part remains stationary as shown in Fig. 4. At the interface, interpolation is calculated by a General Grid Interface (GGI) algorithm. The approach has been thoroughly validated in previous studies using *Fluent* and *OpenFOAM* [2, 4].

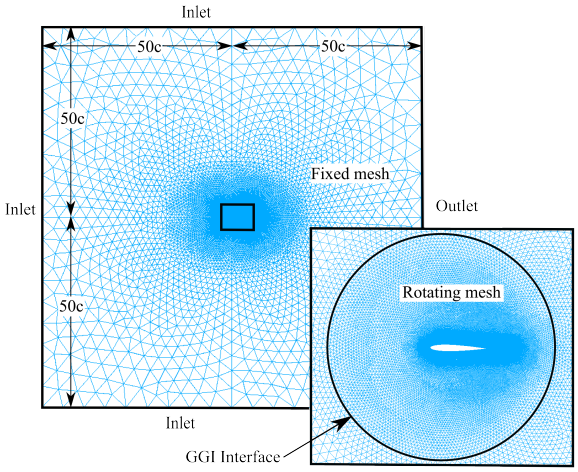

Figure 4: Computational domain and grid details: mesh size $\sim 80,000$ cells.

Varying velocity is imposed at the inlet ($50c$ upstream of the airfoil) and boundaries far above and below the wing to take into account the vertical motion of the airfoil while constant mean static pressure is imposed at the outlet. Acceleration terms are added as body forces in the momentum equation. Adequate near-body resolution (320 cells on both the upper and lower surfaces) is used to capture accurately the vorticity gradients and to satisfy the turbulence model requirement for the first cell thickness, namely $y^+ \leq 1$ on the airfoil surface over the whole cycle [3]. Mesh refinements close to the airfoil in both the streamwise and wall-normal directions have been shown to not influence the results.

3 Results

3.1 Aeroelastic characteristics

Simulations were first performed in order to compare with the experimental results of Mendes *et al.* [5]. The same parameters as in the experiments were used for the inertia, mass, rotation damping, rotational stiffness and heaving stiffness. The heaving damping was first set at $D_h = 3.5$ N·s/m ($\zeta = 0.1$) which was established as an educated guess following a personal communication with Poirel.

To start with, no initial perturbations are imposed. The airfoil was initially at an angle of attack of zero degree with no angular or heaving velocity. Using these initial conditions only small LCOs developed; no large LCOs are obtained. The pitching amplitudes recorded are very similar to the cases where only the pitching motion was allowed (see Fig. 1). The plunging amplitudes are very small, almost negligible. Changing the heaving stiffness from small (75 N/m) to large (371 N/m) has no influence on the results.

The second step was to give the wing an initial perturbation. Providing the wing with an initial heaving velocity ($v_0 = 1$m/s), the results obtained are very different. Using the higher heaving stiffness, LCOs of large pitching and heaving amplitudes are generated. However, when the smaller heaving stiffness is used, no oscillations of significant amplitude occur as in the experiments. Figure 5 presents the pitching and heaving amplitudes as well as frequencies of the large LCOs obtained.

Although the results do not show a good quantitative agreement with the experimental measurements of Mendes *et al.* [5], similar trends are observed. Large pitching amplitudes are obtained over the whole Reynolds number range with both turbulence models as well as in the laminar simulations (no turbulence model added). The numerical simulations also present a decrease in pitching amplitudes at Reynolds numbers higher than $90,000$, a trend also present in the experiments. However the simulations tend to predict higher maximal angles of attack than the experimental measurements.

Frequencies obtained from the computations are quite close to the experiments, albeit slightly higher. Discrepancies between the results can be caused by the turbulence modeling and the two-dimensionnality of the simulations since 2D URANS predictions have a tendency to overestimate the lift due to the artificial vortex coherence in the spanwise direction. It is of interest to note that the frequencies of the two-degrees-

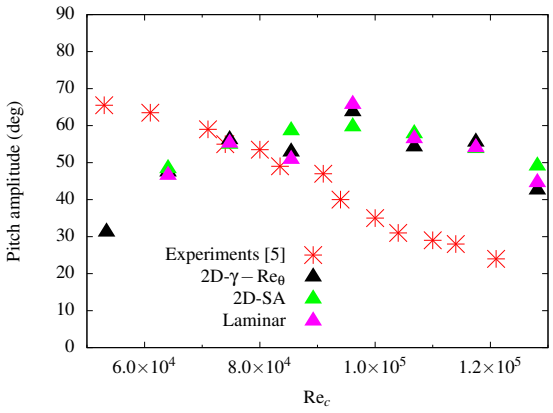

(a) Pitching amplitudes

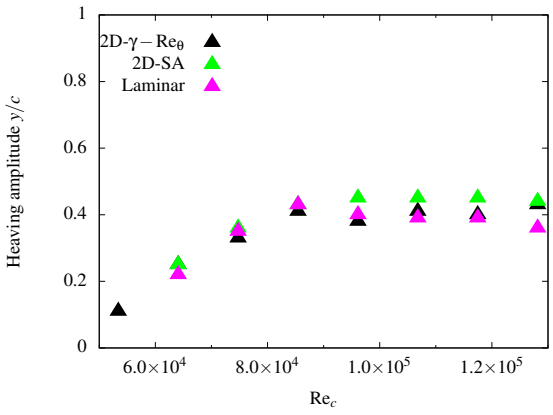

(b) Heaving amplitudes

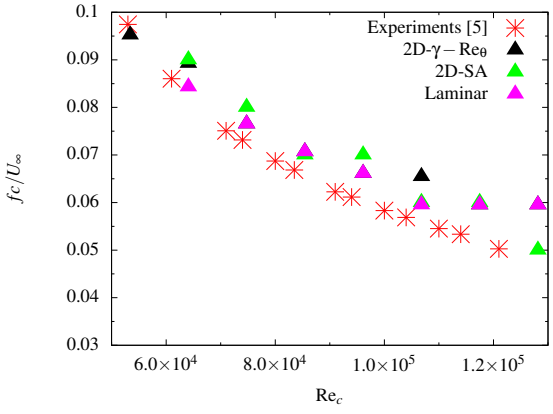

(c) Frequencies

Figure 5: Comparison of self-sustained 2 DOF oscillations characteristics from numerical simulations and experiments.

of-freedom oscillations are very close to those of the pitch-only oscillations despite their different characteristics.

Figures 6 and 7 show the airfoil's pitching and heaving amplitudes at $\mathrm{Re}_c = 75,000$ over the whole run along with the power spectral density of the responses. Both oscillations are periodic and they have the same dominating frequency as expected. This is typical of all cases over the range of Reynolds numbers of interest.

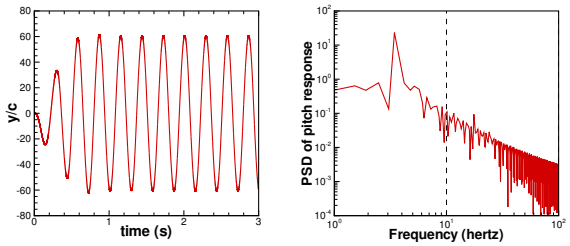

(a) Pitch history (b) PSD of pitch response

Figure 6: Airfoil pitching amplitude and frequency over the whole run at $\mathrm{Re_c} = 75,000$.

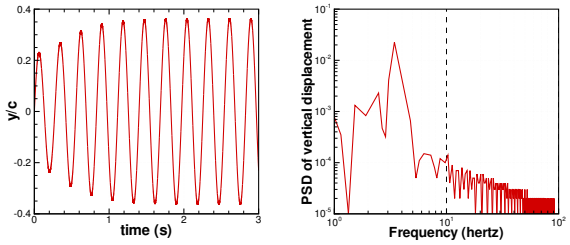

(a) Heaving history (b) PSD of heaving motion

Figure 7: Airfoil heaving amplitude and frequency over the whole run at $\mathrm{Re_c} = 75,000$.

Figure 8 shows both the pitching and heaving response for one LCO cycle at two Reynolds numbers. This shows that there is phase-shift between the pitching and heaving motions as the wing does not reach its higher angle of attack when it is at the highest vertical position. To quantify this phenomenon, ϕ is defined as the phase-shift between the pitching and heaving motions. It is presented in degrees to compare with previous studies even though, in the present case, the motions are not necessarily purely sinusoidal. Hence, for example, $\phi = 90$ degrees corresponds to a shift of a quarter cycle between pitching and heaving.

At $\mathrm{Re_c} = 75,000$ the phase-shift is of 40 degrees ($\sim 1/10$ cycle) while at $\mathrm{Re_c} = 117,500$ it is of 97 degrees ($\sim 1/4$ cycle). Looking over the range of Reynolds numbers, the phase-shift increases with the Reynolds, from 24 degrees at $\mathrm{Re_c} = 64,000$ to 117 degrees at $\mathrm{Re_c} = 139,000$. These results are presented in Table 1.

The evolution of the vertical force coefficient C_y and the aerodynamic moment coefficient C_m in one LCO

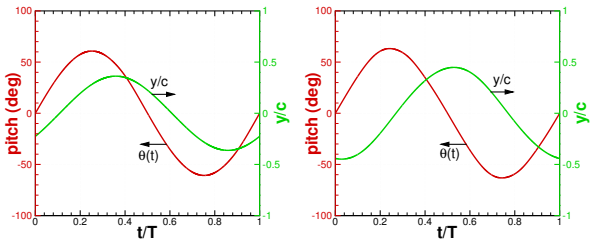

(a) $\mathrm{Re_c} = 75{,}000$ (b) $\mathrm{Re_c} = 117{,}500$

Figure 8: Pitching and heaving responses for one cycle of LCO at two Reynolds numbers.

Re	θ_{max}	$(y/c)_{max}$	fc/U	ϕ
64000	48°	0.25	0.089	26°
75000	55°	0.36	0.076	40°
85500	59°	0.43	0.071	52°
96000	60°	0.45	0.066	72°
107000	58°	0.45	0.059	83°
117500	54°	0.45	0.059	97°
128000	49°	0.44	0.055	108°
139000	45°	0.42	0.055	117°

Table 1: Two DOF self-sustained oscillations characteristics.

cycle is shown in Fig. 9 at the same two Reynolds numbers.

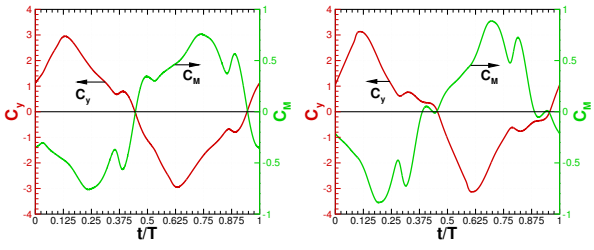

(a) $\mathrm{Re_c} = 75{,}000$ (b) $\mathrm{Re_c} = 117{,}500$

Figure 9: Vertical force and moment coefficients for one cycle of LCO at two Reynolds numbers.

Looking first at C_y, it increases rapidly from $t/T = 0$ to $t = T/8$. Then follows a sharp decrease (up to $t = 3T/8$ at $\mathrm{Re_c} = 75{,}000$ and up to $t = T/4$ at $\mathrm{Re_c} = 117{,}500$) followed by a small plateau slightly above 0 around $t = 3T/8$ and then another decrease to a negative value. The moment coefficient has a somewhat opposite behavior. It is negative and decreasing at the beginning of the cycle and reaches its lower value shortly after C_y reaches its peak. It then increases and goes through a small plateau similar to C_y before increasing to a positive value. For both coefficients the opposite behavior is observed in the second half of the cycle.

3.2 Flow dynamics

The instantaneous spanwise vorticity and pressure contours at eight times in a half-cycle are shown in Figs. 10 and 11 at $\mathrm{Re_c} = 75{,}000$ and $\mathrm{Re_c} = 117{,}500$. The flow dynamics is somewhat similar at both Reynolds numbers. The wing begins its cycle by pitching up, which causes the increase in C_y and decrease of C_m shown in Fig. 9. The pivot point being relatively close to the leading edge, the high angle of attack creates an important negative moment. C_y reaches its peak value around $t = T/8$, when a leading edge vortex starts to appear. This separation of the flow causes deep stall and the rapid decrease of lift from $t = T/8$ to $t = 3T/8$ or $t = T/4$ depending on the Reynolds. C_m reaches its lowest value around $t = T/4$ when the wing is at its highest angle of attack and then increases as the wing starts to pitch down. The small plateau observed in both lift and moment coefficients is caused by a trailing edge vortex that forms around $t = 3T/8$ at $\mathrm{Re_c} = 75{,}000$ and $t = T/4$ at $\mathrm{Re_c} = 117{,}500$. This vortex is bigger at $\mathrm{Re_c} = 117{,}500$ and thus has a sligthly larger impact on the force and moment. At all Reynolds number, a 2P vortex shedding mode [14] is observed as two pairs of vortices are shed in each oscillation cycle.

Contrary to the pitch-only oscillations, laminar separation of the boundary layer is not the triggering phenomenon of the self-sustained pitch-heave oscillations [4, 9]. The large pitch-heave oscillations have been obtained numerically with a fully turbulent model (Spalart-Allmaras) and experimentally even when placing a trip wire close to the leading edge, revealing the secondary role of the boundary layer state. The large oscillations reported here are thus not associated with laminar separation flutter as is the case with the pitch-only oscillations. The LCOs observed here are rather described as coalescence flutter. The instability causing coalescence flutter is due to the coupling between the vertical and torsional degrees of freedom of the airfoil [10]. If the center of gravity of the wing is placed at the pivot point ($x_\theta = 0$ in Eqs. (3) and (4)) then the equations of motion are not coupled and, indeed, simulations performed with this value did not produce any oscillations.

Figures 12 and 13 compare the contours of vorticity and turbulent viscosity ratio (ν_t/ν) between simulations with the Spalart-Allmaras model and simulations

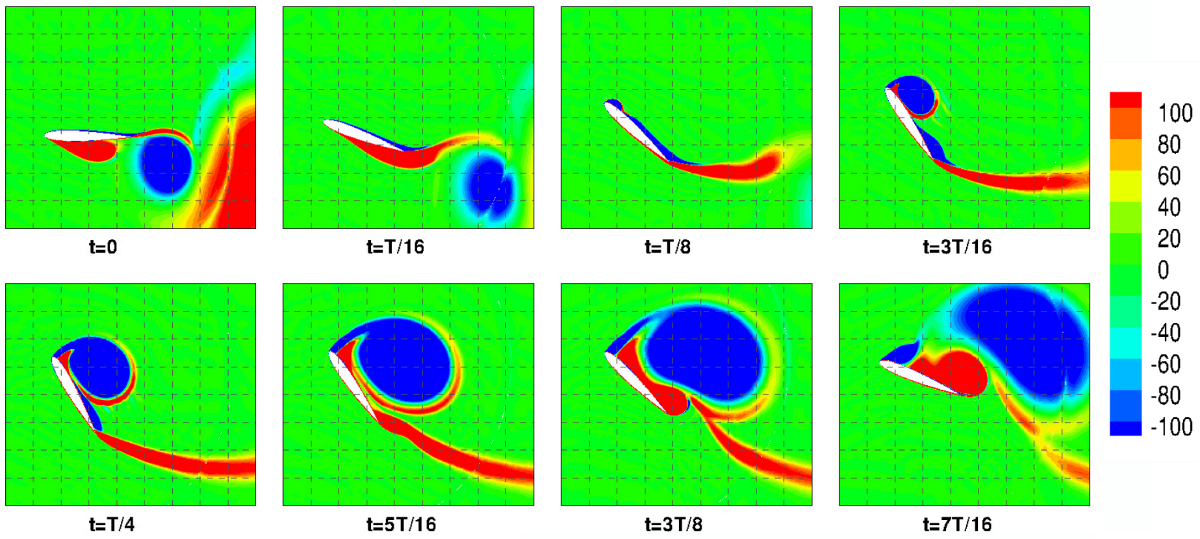

(a) Vorticity contours

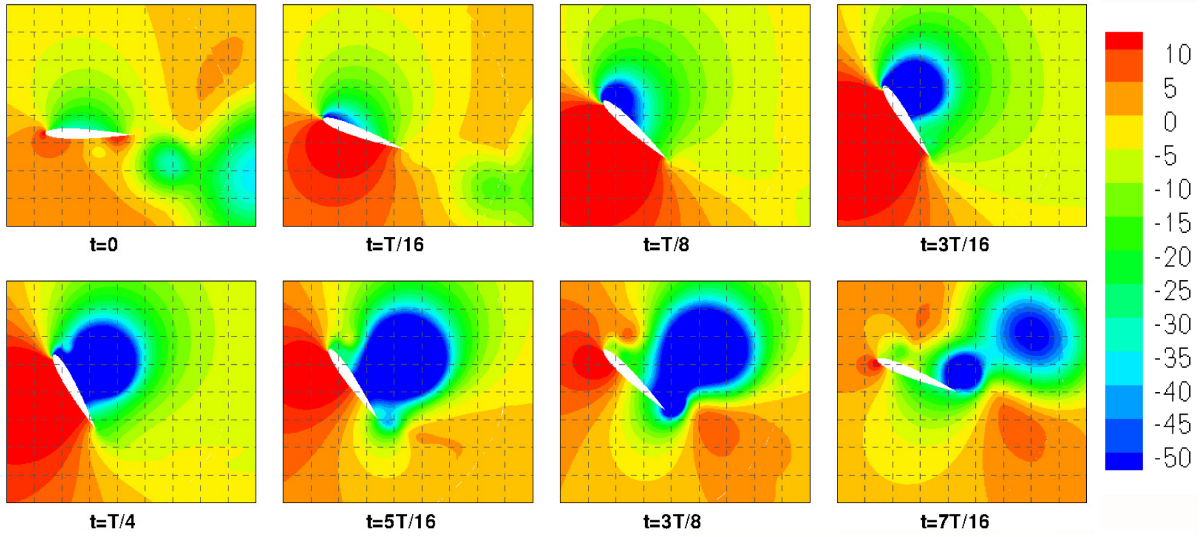

(b) Pressure contours

Figure 10: Instantaneous vorticity and pressure contours at $\mathrm{Re_c} = 75,000$.

with the transition model at the same instant in a cycle at $\mathrm{Re_c} = 75,000$. There are some significant differences in the turbulent viscosity levels between these two simulations as the results obtained with the transition model present lower levels of turbulent viscosity close to the airfoil and in the wake. The flow dynamics observed are somewhat in between those of a laminar simulation and those of the fully-turbulent S-A model. This is reflected in the vorticity contours which show more unsteadiness in the solution computed with the $\gamma - \mathrm{Re}_\theta$ model. Despite this difference in the instantaneous flow fields, the global results are very similar as both models predict similar pitching and heaving amplitudes and frequencies.

4 Conclusion

Self-sustained pitch-heave oscillations of an airfoil have been studied to gain some understanding of the phenomenon. Two-dimensional URANS simulations were performed using both the Spalart-Allmaras and the $\gamma - \mathrm{Re}_\theta$ models. Predicted oscillation frequencies were quite close to the experimental values while pitching amplitudes did not exhibit such a good agreement with the measurements from wind tunnel experiments. However, they still showed comparable trends and similarities. Discrepancies between the numerical and experimental values could be caused by the 2D assumption of the flow which has important impacts in

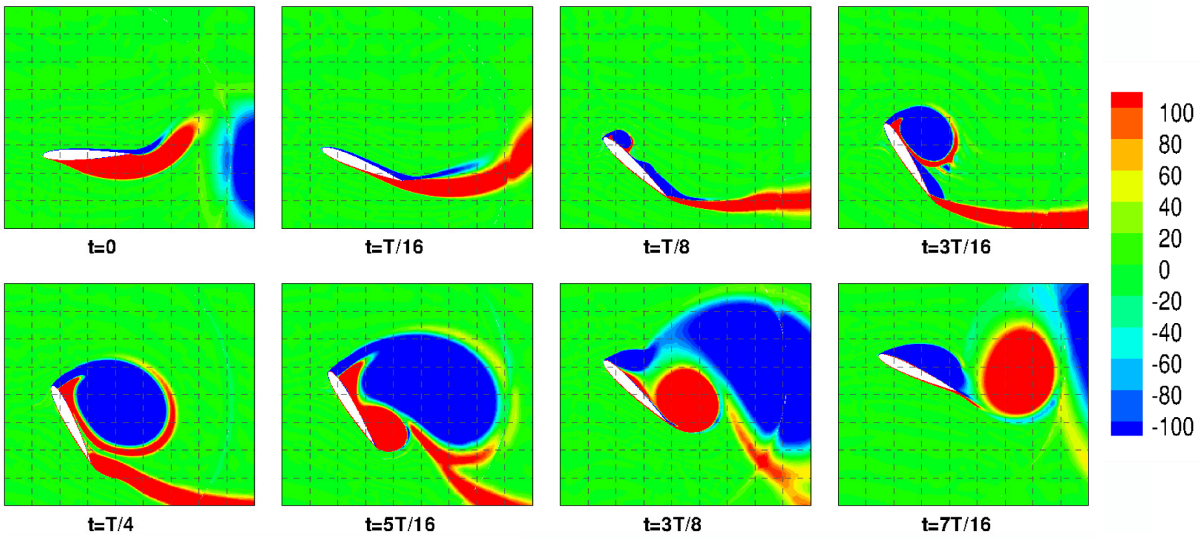

(a) Vorticity contours

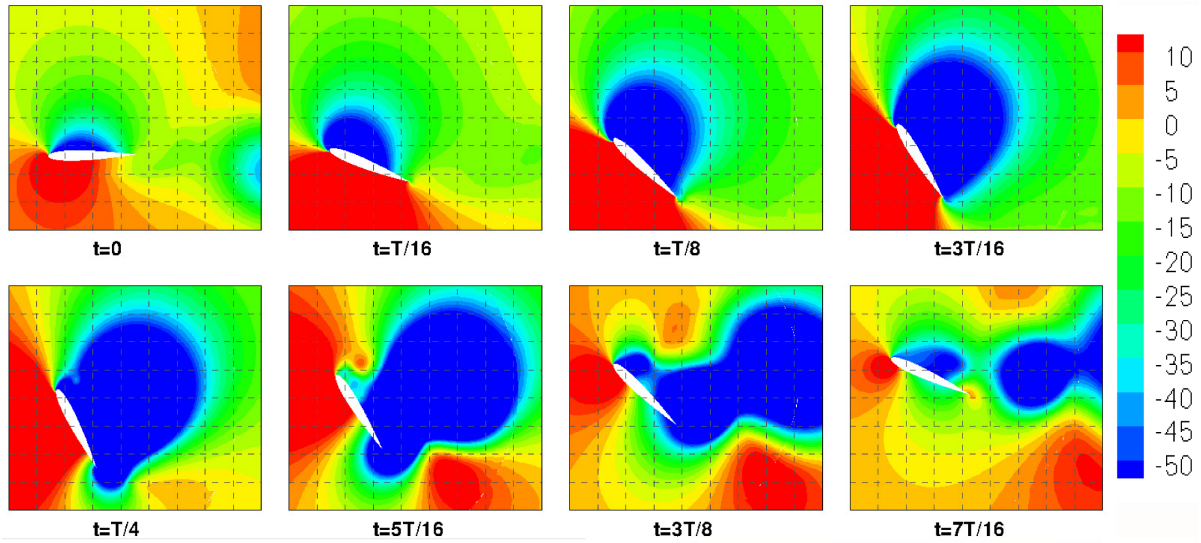

(b) Pressure contours

Figure 11: Instantaneous vorticity and pressure contours at $\mathrm{Re_c} = 117,500$.

the case of massively separated flows.

As opposed to the pitch-only simulations which are caused by laminar separation of the boundary layer, these large oscillations are caused by an instability occuring through the coupling between the pitching and heaving motions and are thus labelled as coalescence flutter. The analysis of the flow fields showed important boundary layer separation at both the leading and trailing edges, causing large vortex shedding.

ACKNOWLEDGEMENTS

Financial support from NSERC Canada and FQRNT Québec is gratefully acknowledged by the authors. Computations were performed on the Colosse supercomputer at the CLUMEQ HPC Consortium and the GPC supercomputer at the SciNet HPC Consortium, both under the auspices of Compute Canada. The authors would also like to thank Prof. D. Poirel for access to his experimental data.

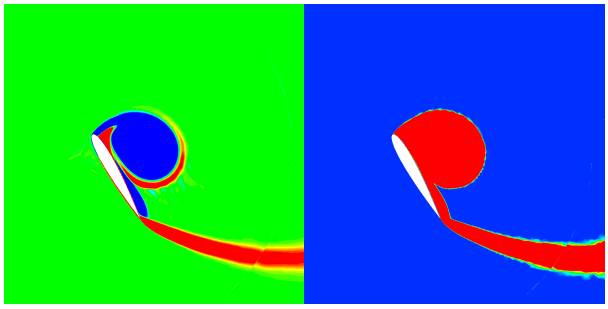

(a) Vorticity contours (b) Viscosity ratio contours

Figure 12: Instantaneous vorticity and turbulent viscosity ratio contours at $\mathrm{Re_c} = 75,000$, Spalart-Allmaras.

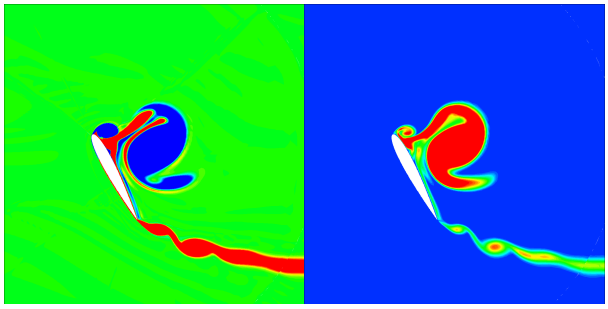

(a) Vorticity contours (b) Viscosity ratio contours

Figure 13: Instantaneous vorticity and turbulent viscosity ratio contours at $\mathrm{Re_c} = 75,000$, $\gamma - \mathrm{Re}_\theta$.

REFERENCES

[1] L. Jones, R. Sandberg, and N. Sandham. Direct numerical simulations of forced and unforced separation bubbles on an airfoil at incidence. *Journal of Fluid Mechanics*, 602:175–207, 2008.

[2] S. Julien, G. Dumas, and V. Métivier. URANS simulations of high amplitude flapping airfoils. Toronto, Canada, May 2007. 15th Annual Conference of the CFD Society of Canada.

[3] R. Langtry. *A Correlation-Based Transition Model using Local Variables for Unstructured Parallelized CFD codes*. PhD thesis, Institute of Thermal Turbomachinery and Machinery Laboratory, University of Stuttgart, 2006.

[4] S. Lapointe and G. Dumas. Improved numerical simulations of self-sustained oscillations of a NACA0012 with transition modeling. *AIAA Paper 2011-3258*, 2011.

[5] F. Mendes, D. Poirel, and A. Benaissa. Experimental investigation of self-sustained pitch-heave aeroelastic oscillations of a NACA0012 airfoil at transitional Reynolds numbers. Montreal, Canada, 2011. CASI 2011.

[6] T. Mueller and J. DeLaurier. Aerodynamics of small vehicles. *Annual Review of Fluid Mechanics*, 35:89–111, 2003.

[7] OpenCFD. *OpenFOAM - The Open Source CFD Toolbox - User's Guide*. OpenCFD Ltd., United Kingdom, 1.5 edition, 1st Aug. 2008.

[8] D. Poirel, Y. Harris, and A. Benaissa. Self-sustained aeroelastic oscillations of a NACA0012 airfoil at low-to-moderate Reynolds numbers. *Journal of Fluids and Structures*, 24(5):700–719, 2008.

[9] D. Poirel, V. Métivier, and G. Dumas. Computational aeroelastic simulations of self-sustained pitch oscillations of a NACA0012 at transitional Reynolds numbers. *Journal of Fluids and Structures*, 27:1262–1277, 2011.

[10] D. Poirel and S. Price. Random binary (coalescence) flutter of a two-dimensional linear airfoil. *Journal of Fluids and Structures*, 18(1):23–42, 2003.

[11] P. Spalart and S. Allmaras. A one-equation turbulence model for aerodynamic flows. *La recherche aérospatiale*, 1:5–21, 1994.

[12] M. Visbal, R. Gordnier, and M. Galbraith. High-fidelity simulations of moving and flexible airfoils at low Reynolds numbers. *Experiments in Fluids*, 46:903–922, 2009.

[13] S. Weber and M. Platzer. Computational simulation of dynamic stall on the nlr 7301 airfoil. *Journal of Fluids and Structures*, 14:779–798, 2000.

[14] C. Williamson and A. Roshko. Vortex formation in the wake of an oscillating cylinder. *Journal of Fluids and Structures*, 2(4):355–381, 1988.